A Simple Proper Orthogonal Decomposition Method for von Karman Plate undergoing Supersonic Flow

Dan Xie[1], Min Xu[2]

Abstract: We apply a simple proper orthogonal decomposition (POD) method to compute the nonlinear oscillations of a degenerate two-dimensional fluttering plate undergoing supersonic flow. First, the von Karman's large deflection theory and quasi-steady aerodynamic theory are employed in constructing the governing equations of the simply supported plate. Then, the governing equations are solved by both the Galerkin method and the POD method. The Galerkin method is accurate but sometimes computationally expensive, since the number of degrees of freedom (dofs) required is relatively large provided that nonlinearity is strong. The POD method can be used to capture the complex dynamics of a strongly nonlinear system using very few degrees of freedom, much fewer than the Galerkin approach. The presently proposed POD method has two advantages over the conventional one. i) a simple numerical difference technique is first introduced to the POD method to avoid the complicated mode-to-mode projection between POD modes and Galerkin modes. ii) POD based reduced order models (POD/ROM) are constructed by using a set of general modes which is extracted from chaotic responses. That is to say POD modes extracted from one set of parameters can be applied to various parameter variations for the same dynamic system. Moveover, results for the buckled, LCO and chaotic responses of the plate are presented and compared with the Galerkin solutions. Numerical examples demonstrate the accuracy and efficiency of the present POD method.

---

[1] College of Astronautics, Northwestern Polytechnical University, Xi'an 710072, P.R. China.
   E-mail: xiedan2151@163.com
[2] College of Astronautics, Northwestern Polytechnical University, Xi'an 710072, P.R. China.

Nomenclature

a_m, b_i	=	nondimensional modal amplitude (Galerkin, POD)
a, b	=	plate length, plate width, m
D	=	plate stiffness, Nm
E	=	Young's modulus, N/m^2
h	=	plate thickness, m
J	=	number of time intervals in a snapshot
L	=	number of modes retained (POD)
l	=	mode number (POD)
M	=	number of modes retained (Galerkin)
m	=	mode number (Galerkin)
Ma	=	Mach number
N	=	number of spatial points in a snapshot
N_x	=	in-plane force (x direction), N/m
$N_x^{(a)}$	=	applied in-plane force (x direction), N/m
P	$\equiv$	$\Delta p a^4 / Dh$
$p - p_\infty$	=	aerodynamic pressure, N/m^2
Δp	=	static pressure differential across the panel, N/m^2
q	=	$\rho U^2/2$, dynamic pressure, N/m^2
$\bar{\mathbf{Q}}$	=	snapshots matrix
R_x	$\equiv$	$N_x^{(a)} a^2 / D$
r, s	=	mode number (Galerkin)
t	=	time, s
U	=	velocity, m/s
$\mathbf{V}$, $\mathbf{v_j}$	=	POD eigenvectors matrix, POD eigenvector
W	$\equiv$	w/h
w	=	plate deflection, m
x, y	=	streamwise, spanwise coordinate, m
β	$\equiv$	$\sqrt{Ma^2 - 1}$
λ	$\equiv$	$2qa^3/\beta D$
λ_j^p	=	POD eigenvalue
μ	$\equiv$	$\rho a/\rho_m h$, fluid/structure mass ratio
ν	=	Poisson ratio
ξ	$\equiv$	x/a
ρ, ρ_m	=	air density, plate density, kg/m^3
σ_x	=	stress
τ	$\equiv$	$t\sqrt{D/\rho_m h a^4}$
Φ, ϕ	=	correlation matrix, Airy stress
Ψ, ψ_i	=	POD modes matrix, POD mode
$(\ )'$, $(\dot{\ })$	=	$\frac{d(\ )}{d\xi}$, $\frac{d(\ )}{d\tau}$
Subscripts		
d	=	dynamic
p	=	peak

1 Introduction

Panel flutter is a self-excitation oscillation with aerodynamic pressure, inertia force and elastic loading functioning together. In linear plate theory, there is a definite flow velocity or dynamic pressure, above which the plate motion becomes unstable, and the response grows rapidly with time, i.e. the plate is in a divergent oscillation. However, in reality, this growing amplitude is limited by the nonlinear induced membrane force, thus we can observe a limit cycle oscillation in the nonlinear panel flutter, in addition, several more complex dynamic oscillations can be observed. The previous work gave a conclusion that the nonlinear panel flutter performs five kinds of oscillation: flat, buckled, LCO, periodic and chaos. Panel nonlinear flutter is common in supersonic flow, although it's not like wing flutter leading to huge damage, yet it can result in fatigue failure, which is also worth of our attention. Therefore, referring to nonlinear panel flutter, many investigations have been carried out.

In early time, Fung (1958) studied the two-dimensional panel flutter and Fung (1960) gave a summery of the theories and experiments on panel flutter. Lock and Fung (1961) studied the nonlinear panel flutter by considering the nonlinear membrane forces induced by the panel motion. Dugundji, Dowell, and Perkin (1963) investigated the subsonic flutter of panels on a continuous elastic foundation. Dugundji (1966) gave the theoretical considerations of panel flutter at high supersonic Mach numbers. Dowell (1966, 1967) studied the nonlinear panel flutter by the use of the Galerkin method. Zhou, Yang, and Gu (2012) applied the Galerkin method to the aeroelastic stability analysis of heated panel with aerodynamic loading on both surfaces. Dai, Paik, and Atluri (2011a,b) applied the global nonlinear Galerkin method for the analysis of elastic large deflections of plates under combined loads and for the solution of von Karman nonlinear plate equations. Dai, Schnoor, and Atluri (2012) proposed a simple collocation scheme to solve nonlinear oscillatory problems, which is promising in solving the von Karman fluttering plate.

To sum up, the nonlinear panel flutter has been investigated for a long time, but almost all of them used the traditional approaches such as Galerkin or Rayleigh-Ritz in common, which as we know are global methods using several given modes to describe the panel deflections. The drawback of them is that in order to obtain relatively accurate solutions, more modes are necessary, especially for larger length-to-width ratios [Dowell (1966); Ye and Dowell (1991)]. At the same time, this kind of global methods can be only employed to analyze simple geometrical plate. For more complex geometrical plate and higher level of accuracy, the finite element method (FEM) is showing up.

By using finite element method, Mei (1977) studied the limit cycle oscillation of a plate in supersonic flow, also Dixon and Mei (1993) explored the nonlinear flutter of rectangular composite panels. Gray and Mei (1993) applied FEM to study the nonlinear flutter characteristics of three-dimensional thin laminated composite panels. Shiau and Kuo (2007) used the FEM with a particular triangle element to study the flutter of thermally buckled composite sandwich plate. However, limited by the large computational cost of the FEM, which usually has tens of thousands of dofs, nonlinear panel flutter analysis has a special challenge that if one wishes to obtain solutions for many different combinations of structural and fluid parameters, the models should be computationally efficient enough to get the resolutions when various parameters are changed in the design process. Thus considerable attention is given to computational effort savings and also to increasing our insight into the physical property of dynamic systems. To satisfy this necessariness, reduced order model (ROM), as an attractive method in nonlinear dynamics gets into our considerations.

For very high dimensional systems, a simpler modal approach for ROM as developed by Romanowski and Dowell (1996) is available. This approach adapts a methodology from the fields of nonlinear dynamics and signal processing, that is, the proper orthogonal decomposition (POD) method or Karhunen-Loève(KL) modal representation. POD uses an ensemble of data, obtained from simulations or from experiments to build the reduced subspace that contains most information of the original dynamic systems. This method furnishes the best orthogonal basis, which decorrelates the signal components and maximizes variance. The POD method provides a set of basis functions for representing a given data set from which a lower-dimensional subspace can be identified.

The POD method have been applied in many fields. Berkooz, Holmes, and Lumley (1993) along with Kunisch and Volkwein (2002) provide applications of the POD/Galerkin reduced order models for fluid dynamics. Additionally, due to the features of POMs extracted, ROMs based on them have been applied to model updating for nonlinear structural dynamics [Lenaerts, Kerschen, and Golinval (2001); Kerschen and Golinval (2004)]. Amabili, Sarkar, and Paidoussis (2003, 2006) gave the comparisons between the POD method and the Galerkin method for a water-filled circular cylindrical shell. Mortara, Slater, and Beran (2000, 2004) have applied the proper orthogonal decomposition method to panel aeroelastic response. Also Epureanu, Tang, and Paidoussis (2004) explored the coherent structures and their influence on the dynamics of aeroelastic panels with the POD technique.

In the present work, since the deflection in *y*-direction is very small compared to that in *x*-direction, a degenerate simply supported plate undergoing supersonic flow is investigated. The von Karman plate theory and the quasi-steady aerodynamic

theory are employed to construct the governing equations. Because analytical POD modes are not available, numerical difference technique is applied to approximate the differential of POD modes. Then a simple POD technique is proposed to set up the reduced order models with a set of general POD modes, which are extracted from the chaotic response solutions with the Galerkin method. Some numerical examples are performed, which turn out that the POD modes are similar to panel deflection shape. Moreover, the POD method compared favorably with the Galerkin approach in terms of its accuracy and efficiency. Finally some conclusions are drawn in Section 4.

2   Theory analysis

2.1   *Basic equations for two-dimensional nonlinear oscillation plate*
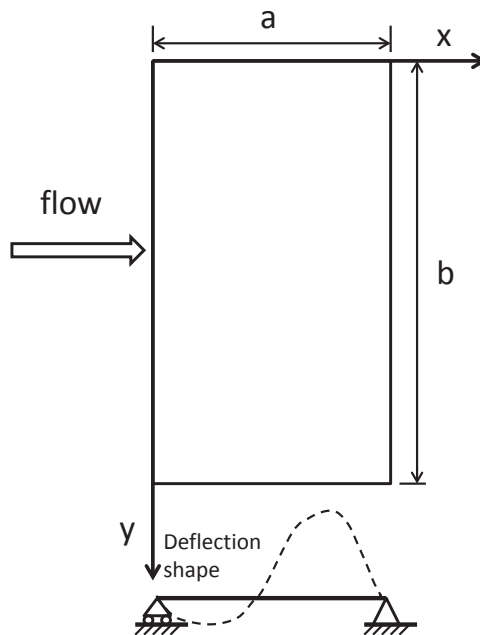
Figure 1: Geometry of degenerate two-dimensional plate.

For a two-dimensional plate undergoing supersonic flow shown in Fig. 1, the original form of von Karman's large deflection equations is

$$D(\frac{\partial^4 w}{\partial x^4} + 2\frac{\partial^4 w}{\partial x^2 \partial y^2} + \frac{\partial^4 w}{\partial y^4}) = q + h(\frac{\partial^2 \phi}{\partial y^2}\frac{\partial^2 w}{\partial x^2} + \frac{\partial^2 \phi}{\partial x^2}\frac{\partial^2 w}{\partial y^2} - 2\frac{\partial^2 \phi}{\partial x \partial y}\frac{\partial^2 w}{\partial x \partial y}), \quad (1)$$

$$\frac{\partial^4 \phi}{\partial x^4} + 2\frac{\partial^4 \phi}{\partial x^2 \partial y^2} + \frac{\partial^4 \phi}{\partial y^4} = E[(\frac{\partial^2 w}{\partial x \partial y})^2 - \frac{\partial^2 w}{\partial x^2}\frac{\partial^2 w}{\partial y^2}]. \tag{2}$$

Eq. (1) is the equilibrium equation of plate, and Eq. (2) is the compatibility equation. For the degenerate two-dimensional plate, there is no spanwise bending, so the deflection in y-direction can be ignored. In that case, $\partial w/\partial y \equiv 0$, $\partial^2 w/\partial y^2 \equiv 0$, and thus the von Karman's equations can be abbreviated as

$$D\frac{\partial^4 w}{\partial x^4} = q + h\frac{\partial^2 \phi}{\partial y^2}\frac{\partial^2 w}{\partial x^2}, \tag{3}$$

$$\frac{\partial^4 \phi}{\partial x^4} + 2\frac{\partial^4 \phi}{\partial x^2 \partial y^2} + \frac{\partial^4 \phi}{\partial y^4} = 0. \tag{4}$$

Considering the applied in-plane load $N_x^{(a)}$, nonlinear induced loading, inertial loading, aerodynamic pressure loading, and static pressure differential across the panel, the Eq. (3) can be rewritten as

$$D\frac{\partial^4 w}{\partial x^4} - [N_x + N_x^{(a)}]\frac{\partial^2 w}{\partial x^2} + \rho_m h\frac{\partial^2 w}{\partial t^2} + (p - p_\infty) = \Delta p, \tag{5}$$

where

$$N_x = Eh/2a \int_0^a (\partial w/\partial x)^2 dx. \tag{6}$$

Using quasi-steady supersonic theory, the aerodynamic pressure loading will be

$$p - p_\infty = \frac{2q}{\beta}[\frac{\partial w}{\partial x} + (\frac{Ma^2 - 2}{Ma^2 - 1})\frac{1}{U}\frac{\partial w}{\partial t}]. \tag{7}$$

Substituting Eq. (6) and Eq. (7) into Eq. (5) and using suitable non-dimensionalization by Dowell (1966), we can yield

$$\frac{\partial^4 W}{\partial \xi^4} - 6(1 - v^2)[\int_0^1 (\frac{\partial W}{\partial \xi})^2 d\xi]\frac{\partial^2 W}{\partial \xi^2} - R_x\frac{\partial^2 W}{\partial \xi^2} + \frac{\partial^2 W}{\partial \tau^2} +$$
$$\lambda[\frac{\partial W}{\partial \xi} + (\frac{Ma^2 - 2}{Ma^2 - 1})(\frac{\mu}{Ma\lambda})^{1/2}\frac{\partial W}{\partial \tau}] = P. \tag{8}$$

In addition to the panel deflection, the stress in the panel is given by

$$\sigma_x = \frac{E}{1 - v^2}(-z\frac{\partial^2 w}{\partial x^2}) + \frac{N_x}{h} + \frac{N_x^{(a)}}{h} = E[\frac{-z}{1 - v^2}\frac{\partial^2 w}{\partial x^2} + \frac{1}{2a}\int_0^a (\frac{\partial w}{\partial x})^2 dx + \frac{N_x^{(a)}}{Eh}]. \tag{9}$$

And in a nondimensional form,

$$\bar{\sigma}_x = \frac{\sigma_x(1 - v^2)}{E(h/a)^2}. \tag{10}$$

2.2 The Galerkin method

The Galerkin method, employing any set of basis functions φ_i, approximates the nonlinear partial differential equations (PDEs) by transforming them into a finite set of coupled ordinary differential equations (ODEs), with the solution being expressed as an expansion of the basis. For a two-dimensional simply supported plate, we assume the trial functions as

$$W(\xi, \tau) = \sum_{m=1}^{M} a_m(\tau) \sin(m\pi\xi), \tag{11}$$

where M is the number of generalized coordinates, i.e. the number of basis functions assumed. The sine function that has an orthogonal property plays the role of basis in the expansion which makes the computation process easier.

By using the Galerkin method, a set of M second-order, ordinary, coupled nonlinear differential equations is obtained for the unknown amplitudes $a_m(\tau)$ of the basis, by successively weighting the original Eq. (8) with each basis $\sin(r\pi\xi)$ retained in Eq. (11) ($r = 1, 2, \cdots, M$) and integrating along the panel length. The resulting ODEs read

$$a_r \frac{(r\pi)^4}{2} + 6(1-v^2)[\sum_m a_m^2 \frac{(m\pi)^2}{2}]a_r \frac{(m\pi)^2}{2} + R_x a_r \frac{(m\pi)^2}{2} + \frac{1}{2}\frac{d^2 a_r}{d\tau^2} +$$

$$\lambda\{\sum_m^{m\neq r} \frac{rm}{r^2-m^2}[1-(-1)^{r+m}]a_m + \frac{1}{2}(\frac{\mu}{Ma\lambda})^{1/2}\frac{da_r}{d\tau}\} = P\frac{1-(-1)^r}{r\pi}; \quad r = 1, 2, \cdots, M. \tag{12}$$

We can solve Eq. (12) by direct numerical integration method, such as 4-th Runge Kutta (RK4). The nondimensional maximum and minimum stresses at $z = \pm h/2$, $y = b/2$ read

$$\bar{\sigma}_x = \frac{\sigma_x(1-v^2)}{E(h/a)^2} = [\pm\frac{1}{2}\sum a_m(m\pi)^2\sin(m\pi\xi) + \frac{1-v^2}{4}\sum a_m^2(m\pi)^2] + \frac{R_x}{12}. \tag{13}$$

2.3 The proper orthogonal decomposition method

The POD method optimally extracts the necessary spatial information to characterize the spatio-temporal complexity and inherent dimension of a dynamic system, from a set of temporal snapshots of the response gathered from, in this paper, the classical Galerkin method. After obtaining POD modes, the solutions from the POD method are compared with the Galerkin solutions.

Rewrite the original ODEs of Eq. (8) in another form

$$W'''' - 6(1-v^2)[\int_0^1 (W')^2 d\xi]W'' - R_x W'' + \frac{\partial^2 W}{\partial \tau^2} +$$

$$\lambda\{W' + (\frac{Ma^2-2}{Ma^2-1})(\frac{\mu}{Ma\lambda})^{1/2}\frac{\partial W}{\partial \tau}\} = P. \quad (14)$$

First, we calculate $W(\xi,\tau)$ at some discrete time points with the Galerkin method , i.e. "snapshots", via which we can construct snapshots matrix:

$$\bar{\mathbf{Q}} = \begin{bmatrix} W(\xi_1,\tau_1) & W(\xi_1,\tau_2) & \cdots & W(\xi_1,\tau_J) \\ W(\xi_2,\tau_1) & W(\xi_2,\tau_2) & \cdots & W(\xi_2,\tau_J) \\ \vdots & \vdots & \ddots & \vdots \\ W(\xi_N,\tau_1) & W(\xi_N,\tau_2) & \cdots & W(\xi_N,\tau_J) \end{bmatrix} \quad (15)$$

where $W(\xi_i,\tau_j)$ denotes the non-dimensional deflection of i-th point in x-direction at j-th time point ($i = 1, 2, \cdots, N; \ j = 1, 2, \cdots, J$). Note that the total number of time points is J, and N is the number of degrees of freedom ($J \ll N$). Now form the correlation matrix for the POD method:

$$\Phi = \bar{\mathbf{Q}}^{\mathbf{T}}\bar{\mathbf{Q}}. \quad (16)$$

Then the following eigenvalue problem is obtained:

$$\Phi\mathbf{v_j} = \lambda_j^p \mathbf{v_j}, \quad (17)$$

where λ_j^p, $\mathbf{v_j}$ ($j = 1, 2, \cdots, J$) are the eigenvalues and eigenvectors of Φ respectively. Resort the eigenvalues in decreasing order and the corresponding eigenvectors $\mathbf{v_j}$ are resorted according to eigenvalues,

$$\lambda_1^p \geqq \lambda_2^p \geqq \cdots \geqq \lambda_J^p.$$

A commonly used criterion for choosing L, the optimal number of basis retained in POD subspace, is the so-called energy contribution criterion. For a predefined "energy percentage" $\varepsilon > 0$, usually let $\varepsilon = 0.999$, then L is chosen by

$$F(k) = \frac{\sum_{k=1}^L \lambda_k^p}{\sum_{j=1}^J \lambda_j^p} \geqq 0.999.$$
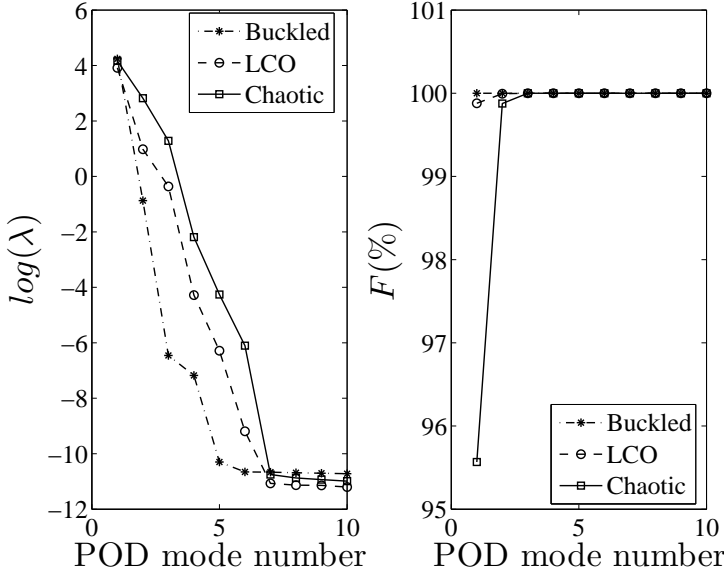
Figure 2: Eigenvalues and the energy percentage versus the number of POD mode.

In that case, the final subspace of POD method is reduced into a lower dimension L, which indicates the number of dominant POMs retained in the POD/ROM. Generally, L is significantly lower than M in Eq. (11) necessary for the Galerkin method. By plotting eigenvalues and energy percentage F as a function of k, we can find that the eigenvalues decrease in a rapid way as the number of eigenvalue and the first several POMs absorb practically all the plate energy, see Fig. 2. So only few dominant modes are employed in the POD/ROM for analysis. Therefore the modal vectors of the correlation matrix are $\mathbf{V} = [\mathbf{v_1},\ \mathbf{v_2},\ \cdots,\ \mathbf{v_L}]$, and then the snapshots are then linearly combined to form a smaller number of basis vectors ψ_i ($i = 1,\ 2,\ \cdots,\ L$), and in matrix form

$$\Psi = \bar{\mathbf{Q}}\mathbf{V}. \tag{18}$$

Now the Ψ are so-called POD modes. It can describe the deflection shape of the plate very well. See Fig. 3 for example.

With the POD modes, we can rewrite the non-dimensional deflection $W(\xi,\tau)$ in a POD expansion form

$$W(\xi,\tau) = \sum_{i=1}^{L} b_i(\tau)\psi_i(\xi). \tag{19}$$

Substituting Eq. (19) into Eq. (14), a set of L coupled second order ODEs about
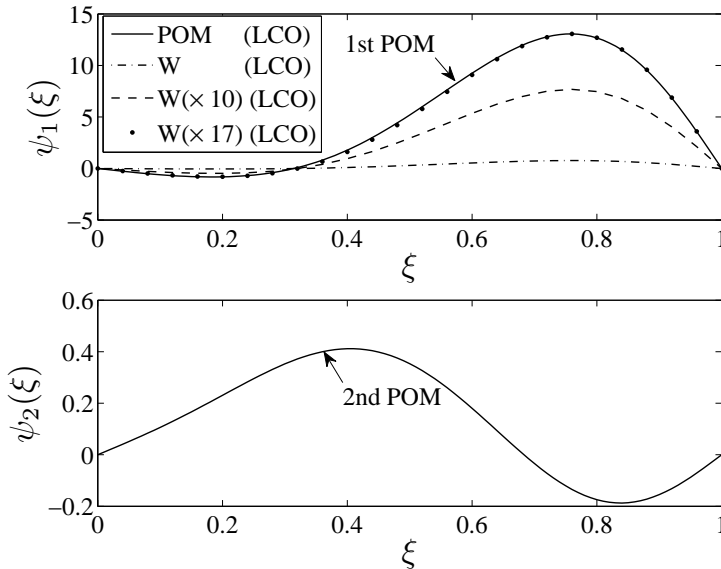
Figure 3: POD modes versus panel deflection shape, take limit cycle oscillation as an example.

coefficients $b_i(\tau)$ can be yielded:

$$\sum_{i=1}^{L} b_i \psi_i'''' - 6(1-v^2) \sum_{j=1}^{N-1} [\sum_{i=1}^{L} b_i \psi_i'(\xi_j)]^2 d\xi \sum_{i=1}^{L} b_i \psi_i'' - R_x \sum_{i=1}^{L} b_i \psi_i'' + \sum_{i=1}^{L} \ddot{b}_i \psi_i +$$

$$\lambda [\sum_{i=1}^{L} b_i \psi_i' + (\frac{Ma^2 - 2}{Ma^2 - 1})(\frac{\mu}{Ma\lambda})^{1/2} \sum_{i=1}^{L} \dot{b}_i \psi_i] = P. \quad (20)$$

In the conventional POD method, expressions of ψ', ψ'', ψ'''' are required to solve Eq. (20) to determine coefficients b_i. However, the POD modes here are numerical data sets, analytical expressions of which are not available to get the differentials. Usually, mode-to-mode projection between the numerical POD mode and the analytical Galerkin mode is implemented. Whereas, the projection procedure requires complicated algebraic derivation and also this procedure costs a large amount of computational effort. To eliminate the mode-to-mode projection, we employ the

numerical difference technique to get the spatial derivative as follows:

$$\psi'(\xi) = \frac{d\psi}{d\xi} = \frac{\psi(\xi + d\xi) - \psi(\xi - d\xi)}{2d\xi},$$

$$\psi''(\xi) = \frac{d^2\psi}{d\xi^2} = \frac{\psi'(\xi + d\xi) - \psi'(\xi - d\xi)}{2d\xi},$$

$$\psi'''(\xi) = \frac{d^3\psi}{d\xi^3} = \frac{\psi''(\xi + d\xi) - \psi''(\xi - d\xi)}{2d\xi},$$

$$\psi''''(\xi) = \frac{d^4\psi}{d\xi^4} = \frac{\psi'''(\xi + d\xi) - \psi'''(\xi - d\xi)}{2d\xi}.$$

Then because of the orthogonality condition $\psi_i^T \psi_j = \lambda_i^p \delta_{ij}$, a set of $2L$ first order ODEs about $b_i(\tau)$ are yielded:

$$\dot{b}_1 = b_{L+1}$$
$$\dot{b}_2 = b_{L+2}$$
$$\vdots$$
$$\dot{b}_L = b_{L+L}$$
$$\vdots$$

$$\dot{b}_{L+i} = \ddot{b}_i = \frac{1}{\lambda_i^p} \{ \psi_i^T [-\sum_{i=1}^{L} b_i \psi_i'''' + \tag{21}$$

$$6(1 - v^2) \sum_{j=1}^{N-1} (\sum_{i=1}^{L} b_i \psi_i'(\xi_j))^2 d\xi \sum_{i=1}^{L} b_i \psi_i'' + R_x \sum_{i=1}^{L} b_i \psi_i''] -$$

$$\lambda \psi_i^T \sum_{i=1}^{L} b_i \psi_i' - \lambda_i^p \lambda (\frac{Ma^2 - 2}{Ma^2 - 1})(\frac{\mu}{\beta\lambda})^{1/2} \sum_{i=1}^{L} b_{L+i} \psi_i + \psi_i^T P \}$$

$$\vdots$$

$$i = 1, 2, \cdots, L.$$

Later on, Eq. (21) can be readily solved by the RK4. Along with the coefficients of POD mode, finally we can compute the deflection and stress. The nondimensional maximum and minimum stresses are

$$\bar{\sigma}_x = \pm\frac{1}{2} \sum_{i=1}^{L} b_i \psi_i'' + \frac{1 - v^2}{2} \sum_{j=1}^{N-1} [\sum_{i=1}^{L} b_i \psi_i'(\xi_j)]^2 d\xi + \frac{R_x}{12}, \tag{22}$$

3   Numerical results and discussions

The simply supported, two-dimensional nonlinear oscillation plate is considered with the following geometrical dimensions and material properties: $a = 2$, $b = 1$, $h = 0.01$; $E = 7.17 \times 10^{10} Pa$, $v = 0.33$.

3.1   The physical property of POD modes

We know that for a simply supported plate, the Galerkin method as a conventional approach commonly used to solve the nonlinear oscillation plate gives the panel deflection in an expression of sine basis. However, the problem is that when the nonlinearity is strong, the Galerkin method has to include more basis functions. Consequently, the resulting ODEs is hard to solve for the larger degrees of freedom (dofs). Considering this drawback, the POD method is applied to construct reduced order models. In the POD method, we seek a general set of proper orthogonal modes, which intrinsically approximates the deflection of the plate. Therefore, for different cases, the same set of POD modes can be employed to compute approximate solutions. Moreover, the number of modes is much less than the dofs of the Galerkin method, which significantly reduces the computational efforts.

Here, taking three typical cases as examples: buckled, LCO and chaotic responses, we compute the snapshots and find the POD eigenvalues. For the sake of brevity, Tab. 1 shows the first 10 POD eigenvalues in the decreasing order; apparently, they decrease in a rapid way, and the dominant eigenvalues are the first few ones, which indicates that the POD method with fewer modes has extracted essential modal information from the snapshots. In this sense, the size of original model can be reduced.

Table 1: First 10 POD eigenvalues in decreasing order for three responses

λ^p	Buckled($\times 10^4$)	LCO($\times 10^3$)	Chaotic($\times 10^3$)
λ_1^p	2.081201786256980	4.998005373311598	9.438495023031926
λ_2^p	0.000006296329819	0.005710978296343	0.487699359764489
λ_3^p	0.000000000015726	0.000258594757087	0.019660255489314
λ_4^p	0.000000000000300	0.000000046915919	0.000004885742612
λ_5^p	0.000000000000004	0.000000002113003	0.000000045487996
λ_6^p	0.000000000000004	0.000000000015824	0.000000000538761
λ_7^p	0.000000000000003	0.000000000000005	0.000000000000008
λ_8^p	0.000000000000003	0.000000000000005	0.000000000000008
λ_9^p	0.000000000000003	0.000000000000005	0.000000000000008
λ_{10}^p	0.000000000000003	0.000000000000004	0.000000000000007

In addition, in order to have a better insight into the physical property of the POD modes, considering the limit cycle oscillation, when $\lambda = 500$, $R_x = 0$, $P = 0$, we compute the deflection at 75% of the chordwise length with the Galerkin method and plot the POD modes and panel deflection shape together for comparison in Fig. 3. Note that 17 times of the response resolution is almost identical with the first POD mode, which indicates that the first POD mode is sufficient to represent the panel deflection. Therefore, reduced order models based on the POD methodology employing better and fewer modes to solve the panel nonlinear oscillation are feasible and encouraging.

3.2   Comparison of the POD and the Galerkin solutions

Herein, as the first consideration, the limit cycle oscillation is analyzed with the POD method. Particularly, the panel deflection shape and stress distribution are computed and the comparison with the Galerkin method is shown in Fig. 4, which shows that for several dynamic pressures, resolutions are compared well between the POD and the Galerkin methods. In addition, the deflection and stress versus nondimensional dynamic pressure are calculated. The comparisons shown in Fig. 5 also obtain a good agreement between the two methods.

For more detailed comparisons between the POD/ROM and the Galerkin method, three typical cases are considered here: buckled, LCO, and chaotic responses. Firstly, the Galerkin solutions are taken as snapshots to construct corresponding POD modes, which in Fig. 6, are labeled "POM", and these three cases have different POMs. Buckled case has only one dominant POM, LCO has two and chaotic has three dominant POMs. Representative comparisons are shown between the Galerkin method and the POD method below. Note that the response in time history is obtained at $\xi = 0.75$.

Two dominant POMs are found and employed to solve LCO case. In Fig. 7(a) the deflection in time history with POD and the Galerkin are plotted together, and as expected, they are in reasonably good agreement with each other. And then Fig. 7(b) shows the generalized coordinates of POMs, which indicate the contribution of each POM to the panel deflection, and they both vary with time in the similar way as deflection with time.

For buckled case, which has only one POM, in order to get the resolution at a better level of accuracy, the three POMs from the chaotic response resolutions via the Galerkin are applied to calculate the deflection response. The results of Fig. 8(a) are in excellent agreement with the Galerkin solutions. In Fig. 8(b), it should be noted that the third generalized coordinate of POM is on an order of 10^{-3}, which is much smaller than that of the first and second coordinates. Hence, we come to the conclusion that, the third POM provides little contribution to the buckled response.
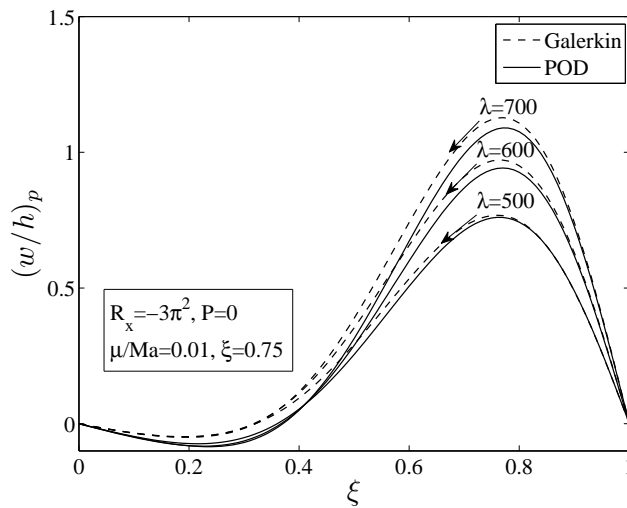
(a)
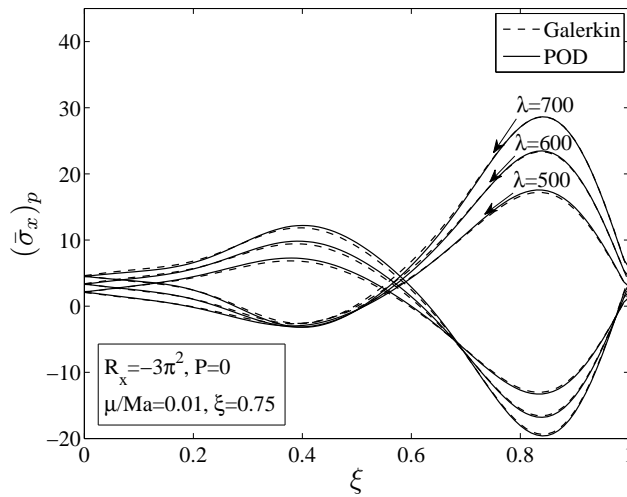
(b)

Figure 4: Comparison between the POD and the Galerkin for several LCO responses: (a) panel deflection shape; (b) panel stress distribution.
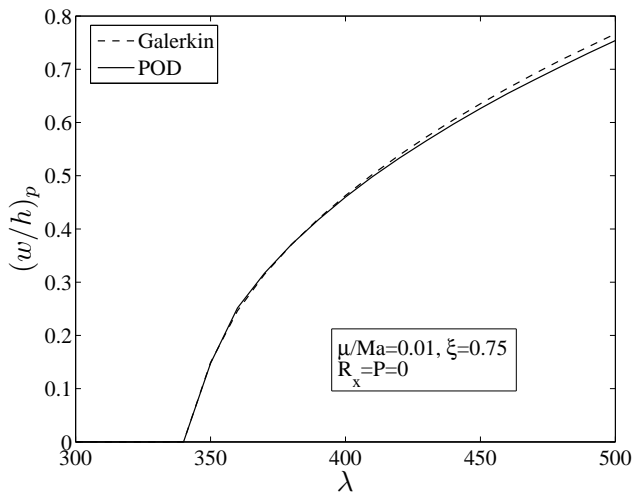
(a)
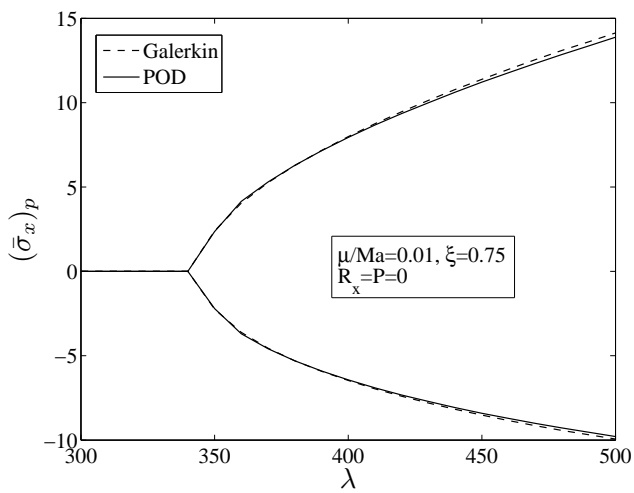
(b)

Figure 5: Comparison between the POD and the Galerkin for LCO amplitude vs λ: (a) panel deflection amplitude vs λ; (b) panel stress amplitude vs λ.
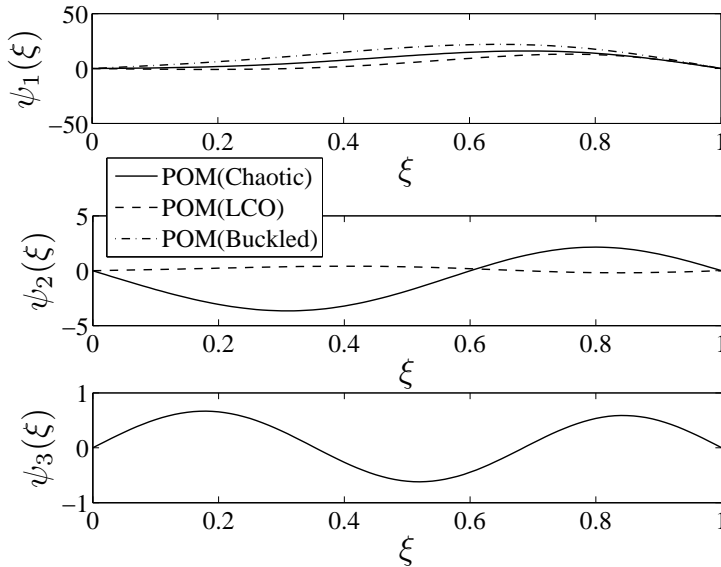
Figure 6: POMs extracted from three different panel responses: chaotic, LCO, buckled.

The results of deflection time response and generalized coordinates versus time for chaotic case in Figs. 9(a) and 9(b) indicate that the chaotic POMs have the richest modal information, which also corroborates the conclusion that the best snapshots to extract POD modes should be the chaotic response by Amabili, Sarkar, and Paidoussis (2006). So in this paper, almost all the computations with the POD method are completed with chaotic POMs.

Finally, from a different perspective and based on the responses above, frequency analysis is performed. As shown in Tab. 2, the first several dominant frequencies of limit cycle oscillation and chaotic responses are calculated. Obviously, a good correlation is obtained between the Galerkin and the POD resolutions. Additionally, the LCO response has two dominant frequencies, and the chaotic response has three, which are totally coincident with the number of dominant POD modes.

Table 2: Dominant frequencies for LCO and chaotic responses

	LCO		Chaotic		
$f(Hz)$	$f1$	$f2$	$f1$	$f2$	$f3$
Galerkin	6.661	19.15	1.665	4.996	7.494
POD	6.656	19.97	1.664	4.992	7.488
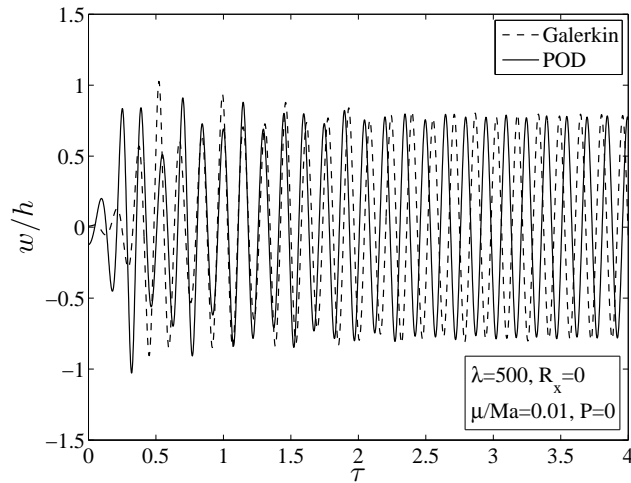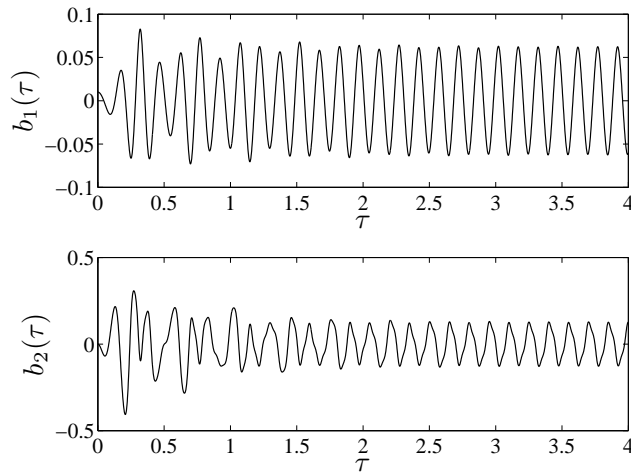
Figure 7: Comparison between the POD and the Galerkin for LCO response: (a) panel deflection time response; (b) generalized coordinates time response.
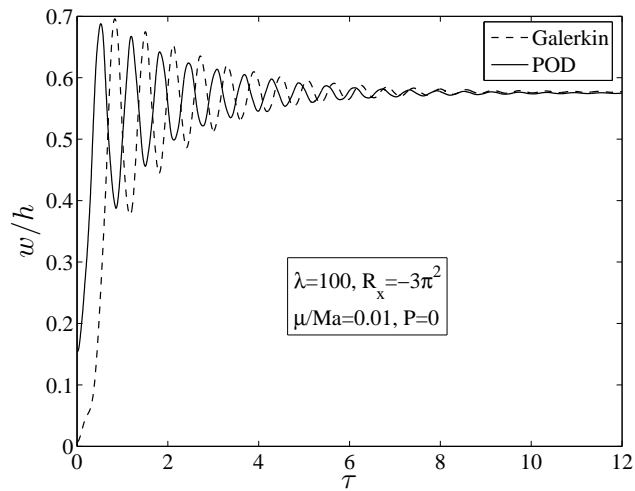
(a)
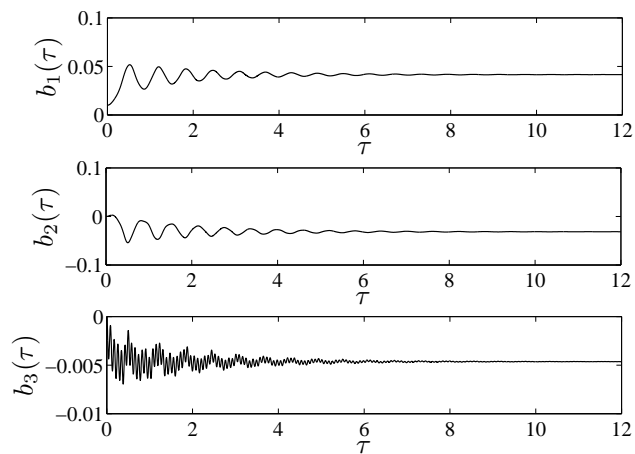
(b)

Figure 8: Comparison between the POD and the Galerkin for buckled response: (a) panel deflection time response; (b) generalized coordinates time response.
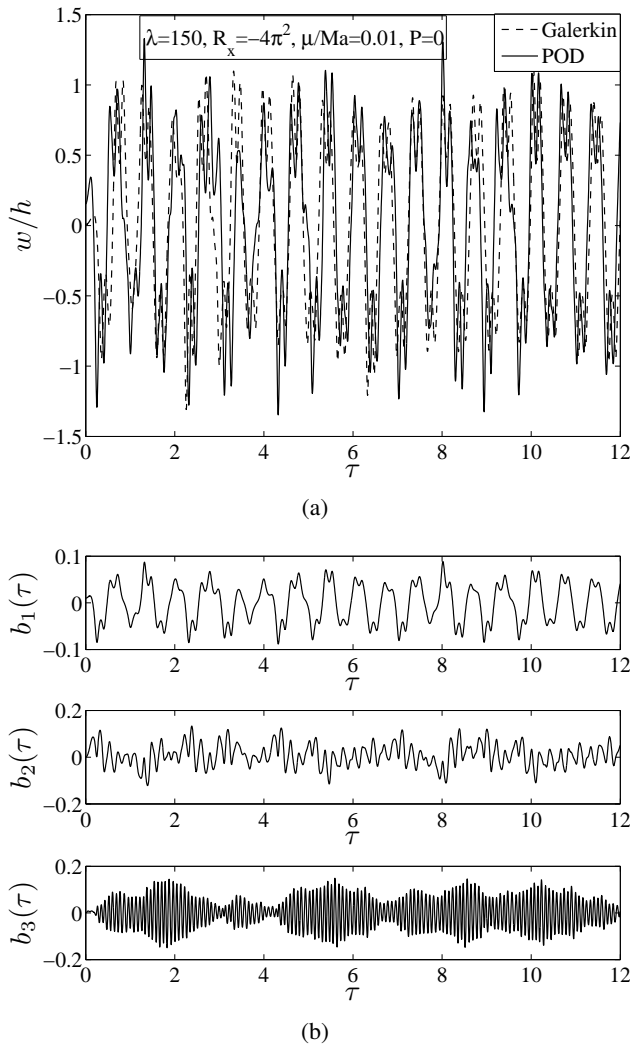
Figure 9: Comparison between the POD and the Galerkin for chaotic response: (a) panel deflection time response; (b) generalized coordinates time response.

3.3 *Effect of applied compressive in-plane load R_x*

In nonlinear large deflection plate theory, there is an induced stretching in-plane load N_x, which is usually coupled with out-of-plane bending, thus the plate amplitudes will generally be limited to a few plate thicknesses. However one can also investigate an applied compressive in-plane load represented by R_x in nondimen-

sional form.

Let $R_x = 0, \ -\pi^2, \ -2\pi^2, \ -3\pi^2$ respectively, and plot peak amplitude versus dynamic pressure λ. In Fig. 10(a), when $R_x < -\pi^2$, there are two branches, one of which is with smaller λ, and the deflection decreases with the dynamic pressure. For another branch with higher λ, however, the amplitude increased with the dynamic pressure. And from Fig. 10(a), it is evident that the intersection of these two branches is at about $R_x = -3\pi^2, \ \lambda = 110$.

Now consider what happens when we plot the steady mean and dynamic LCO amplitudes respectively, and thus a more in-depth interpretation of this behavior is given by Figs. 10(b) and 10(c). Obviously, the steady mean amplitude actually contributes to the first branch of deflection peak in Fig. 10(a), and the dynamic LCO amplitude represents the second branch. The intersections for these three figures are totally the same.

Based on these two branch figures, we know that the smaller λ branch is a nonlinear buckling problem, and the compressive load with largest magnitude has the largest amplitude buckling problem, which indicates that the buckling is mainly produced by in-plane compressive load. However, it is limited by the increasing λ; this can be observed in Fig. 10(b), which indicates that the buckling problem is modified by the aerodynamic flow. And then turn to the second branch, which is obtained with increasing λ; the ever steady mean amplitude has been reduced to zero, as shown in Fig. 10(b); On the other hand, Fig. 10(c) indicates that the dynamic amplitude is starting to increase from zero, which means that the plate has started to transform from buckling to a limit cycle oscillation (nonlinear flutter). The transform often starts differently depending on the distinct in-plane compressive loads calculated, and the branch curve of $R_x = -3\pi^2$ starts first at $\lambda = 110$. Therefore, it is that the in-plane compressive load with largest magnitude has the strongest coupling with the aerodynamic force.

As a concluding discussion, all the results in Figs. 10(a), 10(b) and 10(c) are compared between the Galerkin and the POD methods and they are in excellent agreement with each other.

Now some diverse R_x and λ sets are calculated. Six R_x loads are computed, and for each R_x, three or more dynamic pressure λ are involved. And then the phase portrait of the panel deflection response for these parameter sets are shown in Figs. 11(a)-(f).

Particularly, in phase plane, a teeny circle indicates that the panel is oscillating about zero position with zero frequency, another way said, the plate is flat without oscillation. A standard circle with nonzero displacement and velocity corresponds to limit cycle oscillation. Moreover, a multiple circle with positive displacement
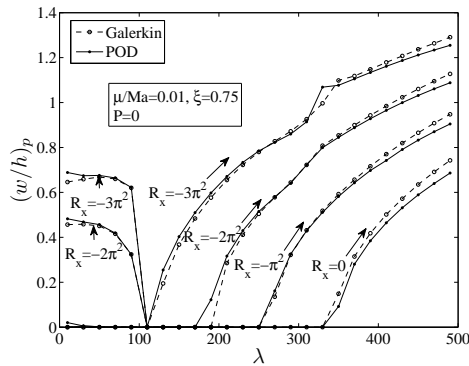
(a)
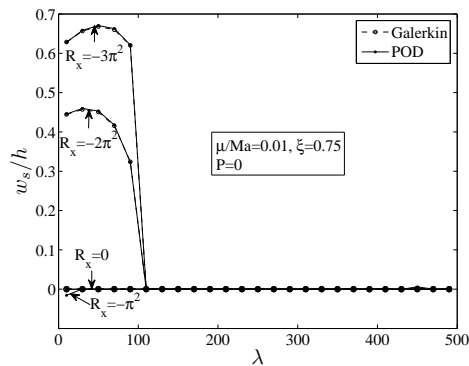
(b)
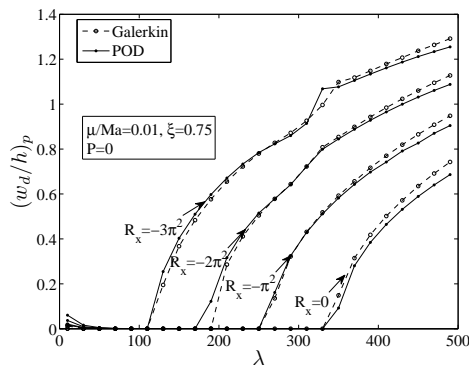
(c)

Figure 10: Comparison between the POD and the Galerkin for limit cycle amplitude versus dynamic pressure: (a) peak amplitude of limit cycle oscillation; (b) steady mean amplitude of limit cycle oscillation; (c) dynamic limit cycle amplitude of limit cycle oscillation.
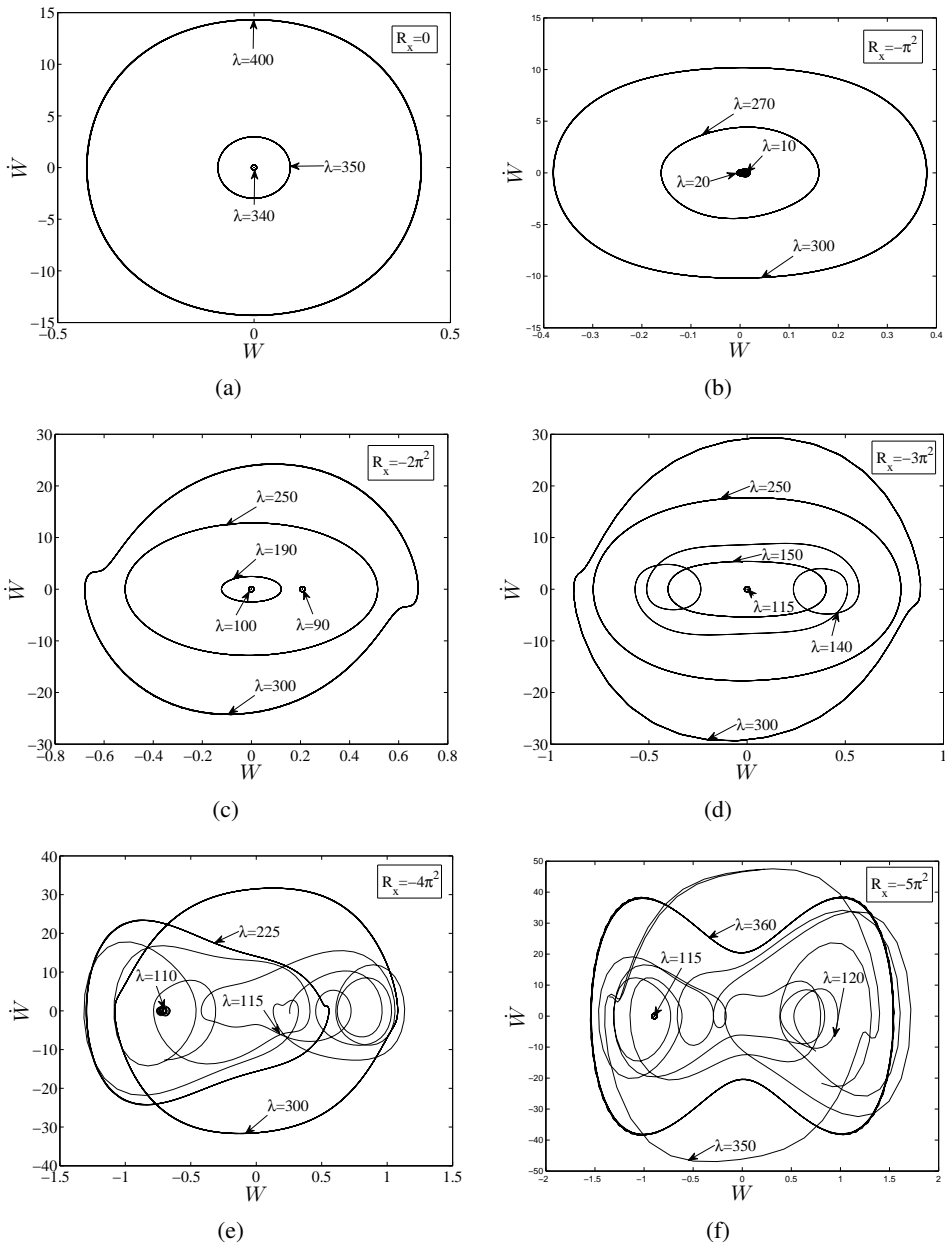
Figure 11: Deflection in phase planes under different in-plane compressive load R_x for several dynamic pressure λ: (a) deflection in phase plane for $R_x = 0$; (b) deflection in phase plane $R_x = -1$; (c) deflection in phase plane for $R_x = -2$; (d) deflection in phase plane for $R_x = -3$; (e) deflection in phase plane for $R_x = -4$; (f) deflection in phase plane for $R_x = -5$.
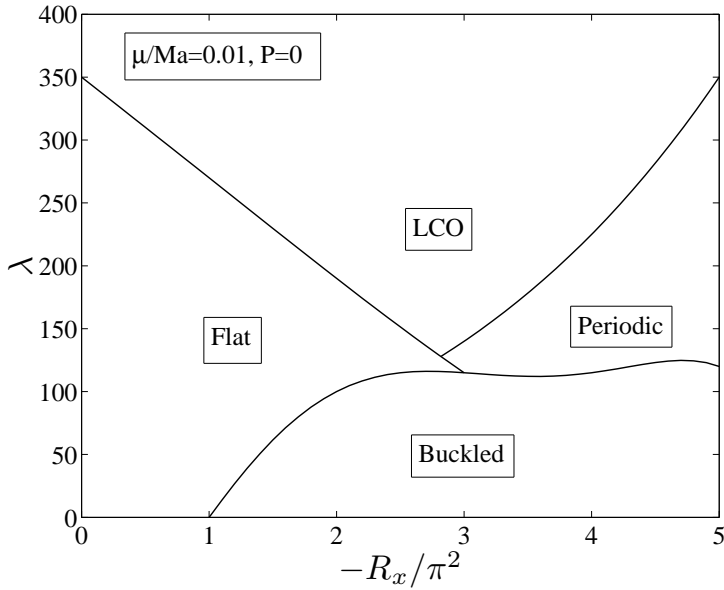
Figure 12: Panel stability regions.
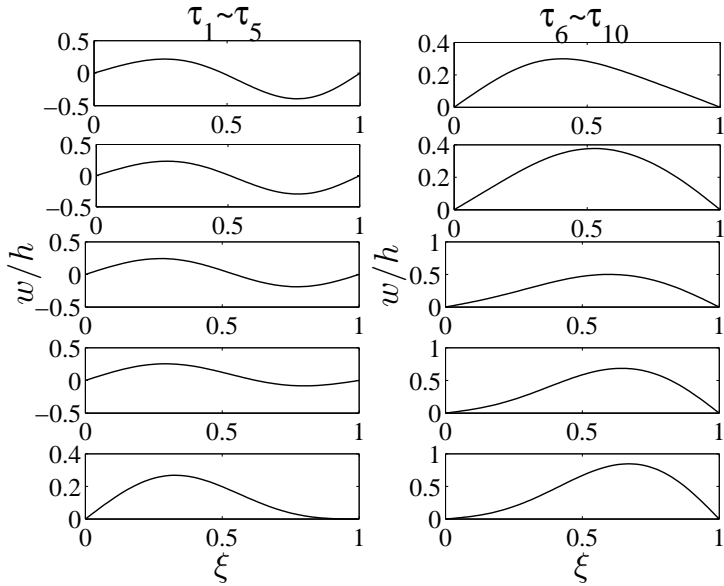
Figure 13: Panel shape during 10 different time of chaotic response for $\lambda = 150$, $R_x = -4\pi^2$, $P = 0$, $\mu/Ma = 0.01$.

and nonzero velocity represents buckling response. In addition, a closed but non-standard circle is periodic motion but not simple harmonic oscillation. Finally, a relatively random and not closed curve corresponds to a chaotic response.

Based on the property above about the phase portrait of different motions for a plate, stability regions boundaries can be found. See Fig. 12, which are in excellent agreement with those given by Dowell (1966), there are four kinds of motion for a nonlinear oscillating plate. It should be noted that the "Periodic" region includes the chaotic and periodic but not simple harmonic responses. These four types of motions have illustrated how the in-plane compressive load and aerodynamic force interact with each other.

At low dynamic pressure and without in-plane load, the plate oscillates about a infinitesimal disturbance and finally becomes statically stable and returns to the initial equilibrium position, as a flat plate. The second motion is LCO, i.e. limit cycle oscillation, with higher λ and still zero R_x; obviously, LCO is produced by the coupling of aerodynamic force and induced in-plane stretching load. The third motion is buckled, with low flow velocity but moderate applied compressive in-plane load; the plate oscillates about a new equilibrium position other than zero as flat, and finally reaches a dynamically stable position with zero frequency oscillation. The last response is quasi-periodic or even chaotic, with moderate dynamic pressure but applied compressive in-plane load with larger magnitude. Then there is a stronger interaction between in-plane compressive load and out-of-plane bending. The plate undergoes a quasi-periodic motion, nearly a kind of chaotic response, which indicates that there is a strong nonlinearity. As an example, $R_x = -4\pi^2$, $\lambda = 150$, the plate goes into chaos as shown in Fig. 13, which is the deflection shape at 10 different time, and there is no apparent periodic property.

3.4 *Effect of static and harmonic pressure differential P*

Physically, when there is a positive pressure differential P, and the dynamic pressure is small enough, the plate will tend to deform upward till it arrives at a static equilibrium position. Then with the increasing dynamic pressure, this static equilibrium position becomes unstable, and thus the plate vibrates about this position till it reaches a new dynamically stable equilibrium motion, which is limit cycle oscillation. However, for a time-dependent pressure differential, e.g. harmonic form, there is a corresponding harmonic response. Especially a critical dynamic pressure can be observed, at which the plate abruptly changes from a low amplitude oscillation to a larger one, i.e. a "jump", which seems like a kind of behavior worth exploring. So considerable discussion about these phenomena are presented below.

First, considering the static pressure differential P, with the increase of P, compute the steady mean and dynamic amplitudes of limit cycle oscillation for several differ-
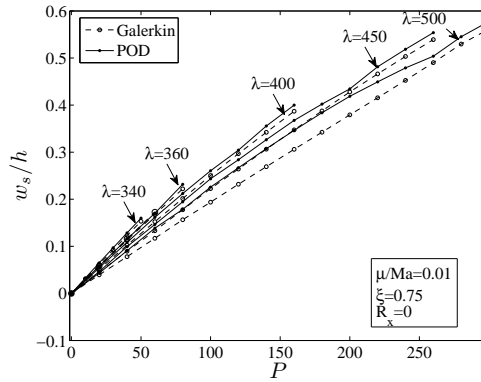
(a)
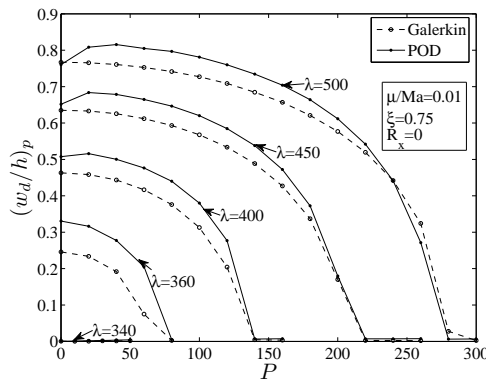
(b)
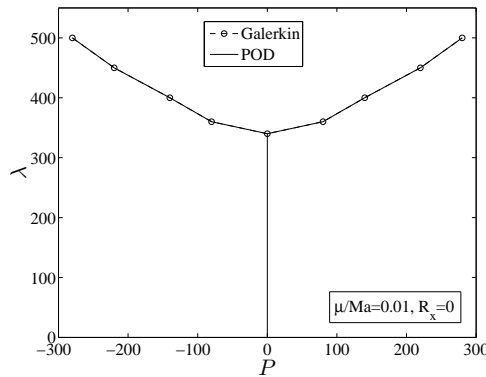
(c)

Figure 14: Comparison between the POD and the Galerkin for constant pressure differential effect to panel response: (a) steady mean amplitude versus static pressure differential; (b) dynamic limit cycle amplitude versus static pressure differential; (c) flutter dynamic pressure versus static pressure differential.
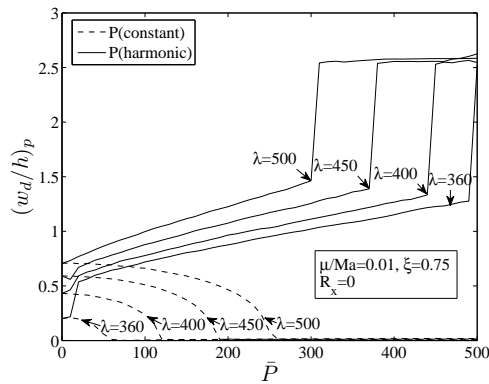
(a)
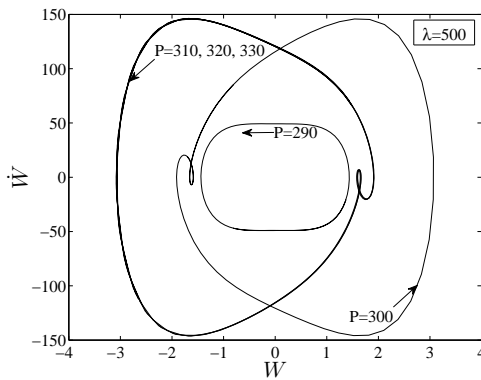
(b)
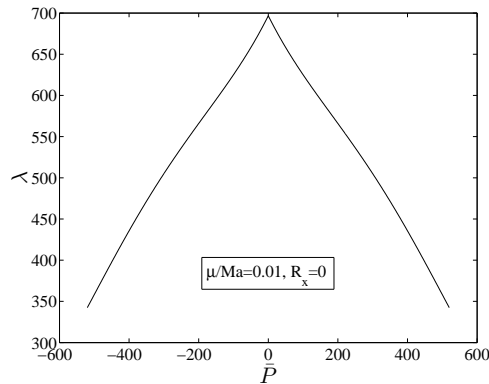
(c)

Figure 15: Harmonic pressure differential effect to panel response: (a) dynamic limit cycle amplitude versus magnitude of harmonic pressure differential; (b) deflection in phase plane for harmonic pressure magnitude $\bar{P} = 500$; (c) jump dynamic pressure versus magnitude of harmonic pressure differential.

ent dynamic pressures. Figs. 14(a) and 14(b) show the comparisons with the POD and the Galerkin methods, and expectedly they compare very well. In addition, with the increasing pressure differential, the steady mean amplitude is increasing, whereas, the dynamic LCO amplitude is decreasing till to zero, which is the critical point for static stability boundary. In Fig. 14(c), this boundary is plotted in terms of λ versus P. The curve is symmetric due to the identical results for P and $-P$, except for the opposite sign of the deflection.

Another interesting case, which is worth of attention, is a harmonic pressure differential, which takes the form as $P = \bar{P}\sin(2\pi ft)$, where $\bar{P}$ is magnitude of pressure differential, and f is frequency of this external excitation. Here let $f = 6.6Hz$, which is about the first natural frequency of the limit cycle oscillation response, as shown in Tab. 2 in Section 3.2.

In order to discuss the different physical phenomena, Fig. 15(a) plots the static and harmonic pressure differential resolutions together. Obviously, compared to the static pressure differential, the dynamic limit cycle amplitude is increasing with the pressure differential amplitude. There is no point at which the dynamic limit cycle amplitude decreases to zero. Whereas, for the harmonic pressure differential, it should be noted that there is a critical point, at which the dynamic limit cycle amplitude has a sudden jump to reach a higher amplitude. The dynamic amplitude after the jump has augmented up to about twice that before the jump.

Additionally, for the sake of a more in-depth interpretation of this jump phenomenon, take $\lambda = 500$ for example, and five $\bar{P}$ are calculated. Phase portrait is shown in Fig. 15(b). For $\bar{P} = 290$, there is a small circle with dynamic amplitude about 1.25; however, for the $\lambda = 300$, there is a larger circle with dynamic amplitude about 2.5, and obviously the circle doubles. Furthermore, with the increasing dynamic pressure $\lambda = 310$, 320, 330, the circles are all the same as the $\lambda = 300$ except the direction. Therefore, the dynamic amplitude after jump does not appear to be much changed. All of these physical phenomena are in agreement with those in Fig. 15(a).

This jump boundary shown in Fig. 15(c) is of interest. We find that the larger dynamic pressure corresponds to the smaller pressure differential magnitude.

The frequency f is also an interesting parameter that affects this jump boundary, the good thing is that, for other frequencies larger than the first natural frequency, there is no jump point, but just a mild trend with increasing $\bar{P}$. Based on the eigenvalues analysis in Section 3.2, the first limit cycle oscillation POM occupies up to 99.88% of the total energy. When the harmonic pressure differential with frequency close to the natural frequency of the lowest POD dominant mode, there is a resonant motion occurring between the harmonic pressure differential and the usual plate limit cycle

oscillation.

3.5   *POD/ROM based on the general POD modes*
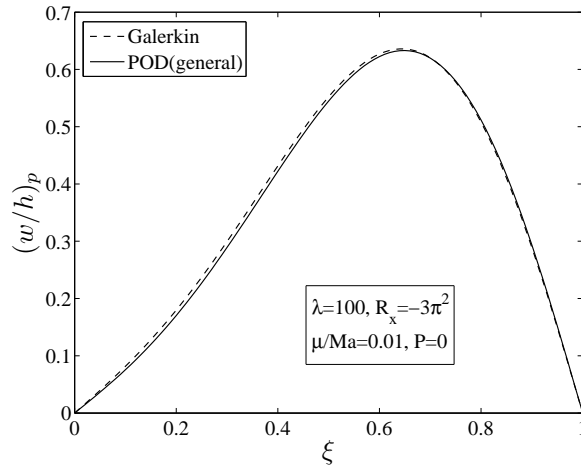
(a)
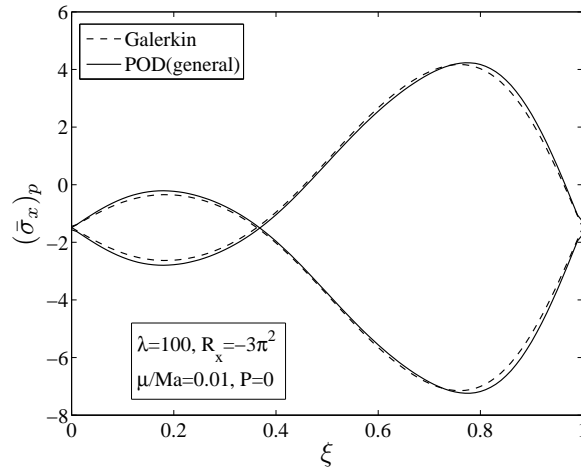
(b)

Figure 16: Comparison between the Galerkin and the POD with general modes for several buckled response: (a) panel deflection shape; (b) panel stress distribution.

It is of interest to investigate the robustness of POD/ROM to variations of the system parameters. Of course it is expected and convenient to use the same set of

POD modes for all cases. POD modes by definition vary with structure/flow conditions, such as, dynamic pressure, in-plane load, pressure differential, and thus the POD modes at one flight condition will not be the modes at another. However, if one can find a general set of POD modes (defined general POMs) that contain most of the modal information of the structure, they will be able to describe accurately the system dynamics at any structure/flow condition. It should be noted that the general POMs, which should contain the richest modal information of the dynamic system, in this paper, are constructed by the Galerkin solution at $R_x = -4\pi^2$, $P = 0$, $\lambda = 150$, i.e. the chaotic response, and this choice has been confirmed by the discussion in Section 3.2. The comparisons of the solutions from the POD with a general set of POMs are provided below to contrast with the Galerkin solutions.

First, a buckled response is calculated using the POD method with general modes. The deflection shape and stress distribution comparisons with the Galerkin method shown in Figs. 16(a) and 16(b) obtain a good agreement, which indicates the ability and the accuracy of the POD method with the general modes. Another example, a plate undergoing the harmonic pressure differential is considered here, where $P = \bar{P}\sin{(2\pi f t)}$, $f = 6.6Hz$. We compute the dynamic limit cycle amplitude by the POD method with the general POMs and the Galerkin method. Fig. 17 gives the
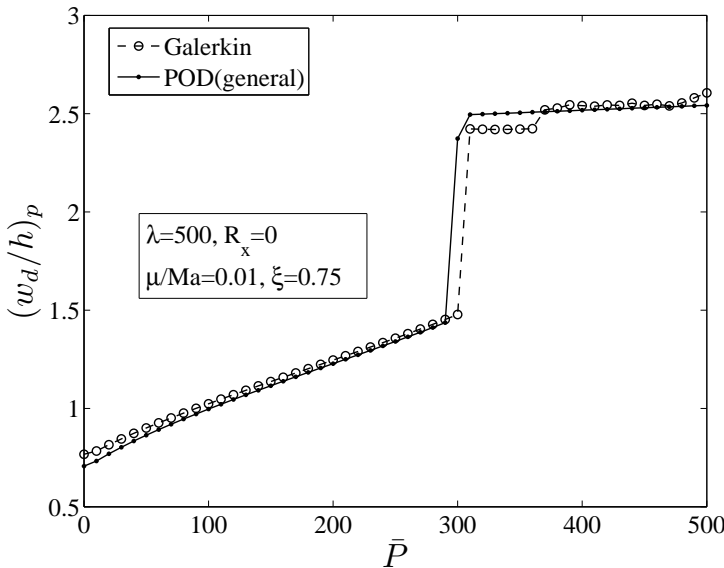
Figure 17: Comparison between the Galerkin and the POD with general POMs for dynamic limit cycle amplitude versus $\bar{P}$.

comparisons, and the solutions from the POD with general POMs are in very good agreement with those from the Galerkin. To sum up, the comparisons demonstrate that the POD with the general POMs can yield exact results under the computational parameters of interest. Furthermore, it is very convenient and efficient for different cases since the general POMs only need to be computed once and for all. Therefore, there are substantially computational savings.

4   Conclusions

In this study, a simple proper orthogonal decomposition approach, using numerical difference technique to get the spatial derivative of the POD modes, is applied to set up the reduced order models with a set of general POD modes, which are extracted from the chaotic response solutions with the Galerkin method. Moreover, the POD method is compared with the Galerkin approach to prove its accuracy and efficiency. The POD method has been employed to analyze the degenerate two-dimensional nonlinear oscillation plate in supersonic flow. Comparing with the classical Galerkin method, the POD modes obtained are similar to the physical deflection shape of the panel, which can better describe the plate physical behavior, so only three or fewer POD modes are necessary to construct the POD/ROM, in that case, fewer ODEs can be obtained compared to those with the Galerkin method, which needs up to 6 modes in the modal representation function. In addition, the computation with the POD method is much faster than that with the Galerkin method. Hence, in the light of better insight into the physical phenomena of structure behavior and computational time savings, the POD method is superior to the Galerkin method. From the discussion of the general POD modes, we know that since the general POD modes extracted from the chaotic response have the richest modal information of the original dynamic system, they are calculated once and can be used for all the parameter sets. Therefore the POD technique has good generality to the variations of the parameter sets. Moreover, the necessary input for the POD method is only a set of data from simulations or experiments; there is no limitation to the plate support conditions. Although a simply supported plate is investigated in the present study, the POD method can be also applied to plates subjected to other support conditions. This makes POD method more universal. Finally, the POD method can be also readily extended to analyze three-dimensional plates.

References

Amabili, M.; Sarkar, A.; Paidoussis, M. P. (2003): Reduced-order models for nonlinear vibrations of cylindrical shells via the proper prthogonal decomposition method. *Journal of Fluids and Structures*, vol. 18, no. 2, pp. 227–250.

Amabili, M.; Sarkar, A.; Paidoussis, M. P. (2006): Chaotic vibrations of circular cylindrical shells: Galerkin versus reduced-order models via the proper orthogonal decomposition method. *Journal of Sound and Vibration*, vol. 290, no. 3, pp. 736–762.

Berkooz, G.; Holmes, P.; Lumley, J. L. (1993): The proper orthogonal decomposition in the analysis of turbulent flows. *Annual Review of Fluid Mechanics*, vol. 25, no. 1, pp. 539–575.

Dai, H. H.; Paik, J. K.; Atluri, S. N. (2011a): The global nonlinear galerkin method for the analysis of elastic large deflections of plates under combined loads: A scalar homotopy method for the direct solution of nonlinear algebraic equations. *Computers Materials and Continua*, vol. 23, no. 1, pp. 69–99.

Dai, H. H.; Paik, J. K.; Atluri, S. N. (2011b): The Global Nonlinear Galerkin Method for the Solution of von Karman Nonlinear Plate Equations: An Optimal & Faster Iterative Method for the Direct Solution of Nonlinear Algebraic Equations $\mathbf{F}(\mathbf{x}) = \mathbf{0}$, using $\mathbf{x} = \lambda[\alpha\mathbf{F} + (1-\alpha)\mathbf{B}^T\mathbf{F}]$. *Computers Materials and Continua*, vol. 23, no. 2, pp. 155–185.

Dai, H. H.; Schnoor, M.; Atluri, S. N. (2012): A simple collocation scheme for obtaining the periodic solutions of the duffing equation, and its equivalence to the high dimensional harmonic balance method: subharmonic oscillations. *Computer Modeling in Engineering and Sciences*, vol. 84, no. 5, pp. 459–497.

Dixon, I. R.; Mei, C. (1993): Finite element analysis of large-amplitude panel flutter of thin laminates. *AIAA Journal*, vol. 31, no. 4, pp. 701–707.

Dowell, E. H. (1966): Nonlinear oscillations of a fluttering plate. *AIAA Journal*, vol. 4, no. 7, pp. 1267–1275.

Dowell, E. H. (1967): Nonlinear oscillations of a fluttering plate. ii. *AIAA Journal*, vol. 5, no. 10, pp. 1856–1862.

Dugundji, J. (1966): Theoretical considerations of panel flutter at high supersonic mach numbers. *AIAA Journal*, vol. 4, no. 7, pp. 1257–1266.

Dugundji, J.; Dowell, E. H.; Perkin, B. (1963): Subsonic flutter of panels on a continuous elastic foundation. *AIAA Journal*, vol. 1, no. 5, pp. 1146–1154.

Epureanu, B. I.; Tang, L. S.; Paidoussis, M. P. (2004):   Coherent structures and their influence on the dynamics of aeroelastic panels. *International Journal of Non-Linear Mechanics*, vol. 39, no. 6, pp. 977–991.

Fung, Y. C. (1958):   On two-dimensional panel flutter.   *Journal of Aeronautical Science*, vol. 25, no. 3, pp. 145–160.

Fung, Y. C. (1960):   A summary of the theories and experiments on panle flutter. *Air Force Office of Scientific Research TN 60-224*.

Gray, C. E.; Mei, C. (1993):   Large-amplitude finite element flutter analysis of composite panels in hypersonic flow.   *AIAA Journal*, vol. 31, no. 6, pp. 1090–1099.

Kerschen, G.; Golinval, J. C. (2004):   A model updating strategy of non-linear vibrating structures. *International Journal for Numerical Methods in Engineering*, vol. 60, no. 13, pp. 2147–2164.

Kunisch, K.; Volkwein, S. (2002):   Galerkin proper orthogonal decomposition methods for a general equation in fluid dynamics.   *SIAM Journal on Numerical Analysis*, vol. 40, no. 2, pp. 492–515.

Lenaerts, V.; Kerschen, G.; Golinval, J. C. (2001):   Proper orthogonal decomposition for model updating of non-linear mechanical systems.   *Mechanical Systems and Signal Processing*, vol. 15, no. 1, pp. 31–43.

Lock, M. H.; Fung, Y. C. (1961):   Comparative experimental and theoretical studies of the flutter of flat panels in a low supersonic flow.   *Air Force Office of Scientific Research TN 670*.

Mei, C. (1977):   A finite-element approach for nonlinear panel flutter.   *AIAA Journal*, vol. 15, pp. 1107–1110.

Mortara, S.; Slater, J.; Beran, P. (2000):   A proper orthogonal decomposition technique for the computation of nonlinear panel response. In *41st Structures, Structural Dynamics, and Materials Conference, Atlanta, Georgia, AIAA-2000-1396*.

Mortara, S.; Slater, J.; Beran, P. (2004):   Analysis of nonlinear aeroelastic panel response using proper orthogonal decomposition. *ASME Journal of Vibration and Acoustics*, vol. 126, no. 3, pp. 416–421.

Romanowski, M. C.; Dowell, E. H. (1996):   Reduced order euler equations for unsteady aerodynamic flows: numerical techniques. *AIAA Pap. 96-0528. Presented at AIAA Aerosp. Sci. Meet. Exhib., 34th, Reno, Nev.*

Shiau, L.; Kuo, S. (2007):   Flutter of thermally buckled composite sandwich plates. *CMC: Computers Materials and Continua*, vol. 5, no. 3, pp. 213–222.

Ye, W. L.; Dowell, E. H. (1991): Limit cycle oscillation of a fluttering cantilever plate. *AIAA Journal*, vol. 29, no. 11, pp. 1929–1936.

Zhou, J.; Yang, Z. C.; Gu, Y. S. (2012): Aeroelastic stability analysis of heated panel with aerodynamic loading on both surfaces. *Science China: Technological Sciences*, vol. 55, pp. 2720–2726.